Transport and Communications Science Journal

HYDRO-MECHANICAL-DAMAGE MODEL FOR THE SECONDARY CREEP OF FIBER REINFORCED MORTAR AT HIGH STRESS-TO-STRENGTH RATIO

Pham Duc Tho[1*], Luca Sorelli [2]

[1]Geotechnical Engineering, Construction Materials and Sustainability – GCMS, Hanoi University of Mining and Geology, Hanoi, Viet Nam

[2]Laval University, Quebec, Canada

[*] *Corresponding author*
Email: phamductho@humg.edu.vn; Tel: +84976415657

Abstract. Recent works have showed that the secondary creep of concrete under sustained high load level of load-to-strength ratio is likely due to a strong coupling between damage and drying shrinkage, which locally occurs in the fracture process zone. The scope of this work is to develop a simplified damage-poromechanical model for the secondary creep of concrete, which directly accounts for such coupling. It was simply assumed that microcracking affects the distribution of the moisture content by scaling the adsorption isotherm with damage. The proposed hydro-mechanical-damage model couplings has been implemented into a discrete lattice method based on dually coupled conduit elements and mechanical element. Notably, the drying shrinkage is accounted within the poromechanical framework of the partially saturated media. The hydro-mechanical-damage model can engender microcrack process zone which govers the secondary creep of concrete at high stress. The model has been validated on 2D experiments of secondary creep on FRC which considers the effect of water-to-cement ratio and aggregate inclusion Finally, the model is validated against experimental results on secondary creep fiber reinforced mortar (FRM) beam considering the effect of concrete heterogeneity.

Keywords: Secondary creep at high stress, damage, adsorption isotherms, hydro-mechanical-damage, microcracking, fiber reinforced concretes.

1. INTRODUCTION

Beyond a certain critical stress-to-strength σ/f_c ratio, creep linearity with respect to the load is lost and its increase is rather exponential. Notably, such threshold value of σ/f_c was found to depend on the concrete heterogeneity, i.e., $\sigma/f_c \sim 0.4$ for concrete and $\sigma/f_c \sim 0.8$ for mortars [1–4]. While the mechanisms associated to concrete creep are still under study [5], there is a general agreement on the role of microcracking on the non-linear creep in both secondary and tertiary phases [6]. For instance, a good experimental correlation between the creep deformation and the acoustic events recorded during a tensile creep test on plain concrete at high stress (with loading level P/P_0 (where P is the load at reloading and P_0 is the load before unloading) in between 54% and 80%)) [7]. At high stress level, creep strains are associated with microcracking growth, which can eventually result in concrete failure by tertiary creep [6]. Thus, deteriorated concrete structures which undergo to excessive creep deformation due to secondary creep may imply an important reduction of the safety coefficient against failure [8].

Rossi et al. [7], [9] claimed that the observed secondary creep concrete under high sustained load level (54-80% of the average compressive strength) is mainly due to an interactive process between microcracking and drying shrinkage. Simply speaking, when the water in the capillary pores of the concrete is drained by dry microcracks, shrinkage strain can occur. If the deformation is locally restrained (ex. by sand/aggregate particles), the internal stress can achieve the tensile strength and causes further micro-cracking.

Based on a recent work on the flexural creep of sealed FRC concrete beams at high loading level (between 60 and 100% of the load required to pre-crack the beam), Rossi et al. [10] showed that the time to failure t_R showed a logarithmic dependence on the loading level, while the secondary creep rate follows a power law with respect to time, i.e., scale invariant. Moreover, the elastic compliance, which was measured by cyclic loading, showed an initial slight decrease up to a certain time, followed by a rapid increase with a logarithmic trend, up to a value after which there is an unstable propagation. This confirms that secondary creep is related to the growth of cracks. Furthermore, Daviau-Desnoyers et al. [11] observed that the failure of the pre-cracked beam reloaded at a certain loading level P/P_0 occurs when the crack opening defined by the static behavior envelope is attained.

In a recent experimental work, digital image correlation was employed to show that the particle heterogeneity can increase the secondary creep of FRC concretes under sustained high load levels [12].

Most of the models proposed for capturing secondary concrete creep are phenomenological. Several models have extended linear visco-elastic model by multiplying the creep compliance by a nonlinear function of the stress-state [13], [14] Bažant et Xiang, 1997 [15] proposed a nonlinear relationship between creep and stress by defining a crack growth as a function of the stress intensity factor. Recent models have accounted for the coupling between creep and damage by introducing a damage law associated to the creep strain [16], [17].

Recently, [18]–[20] implemented a probabilistic lattice model for predicting the flexural creep of concrete beams at high stress. Based on the experimental results they assumed that the time to failure (i.e., the duration of the creep test up to the final collapse) depends exponentially on the stress level

Recently, Pham et al., 2022 [21] showed the ability of a simplified hydro-damage lattice model to predict the secondary creep of FRC beams under high sustained load level [11], [22].

However, the proposed model employed a phenomenological shrinkage coefficient to capture the hydro-mechanical - damage coupling.

The scope of this work is threefold: (i) to develop a new model within the framework of hydro-mechanical – damage coupling that can account for the coupling between microcrack (damage), water diffusion and shrinkage at stake for concrete secondary creep; (ii) to implement it in an existing hydro-damage lattice model [23]; (iii) to validate the model with respect to the flexural creep of Fiber Reinforced Concrete (FRC) and Mortars under high sustained load level [11].

2. HYDRO-MECHANICAL-DAMAGE COUPLING MODEL FOR SECONDARY CREEP OF CONCRETE

2.1 Mechanical - damage lattice model

Recently, a mechanic - damage lattice model has been developed by a random network of Delaunay triangulation and dual Voronoi polygonization. For the mechanical lattice, the elements are placed on the edges of the random Delaunay triangles (Figure 1). The geometry of the cross-section of the lattice elements is determined by the corresponding edge of the Voronoi polygon of length l. Each node has three Degrees of Freedom (DOF): two translations, u and v, and one rotation ϕ.

(a)   (b)
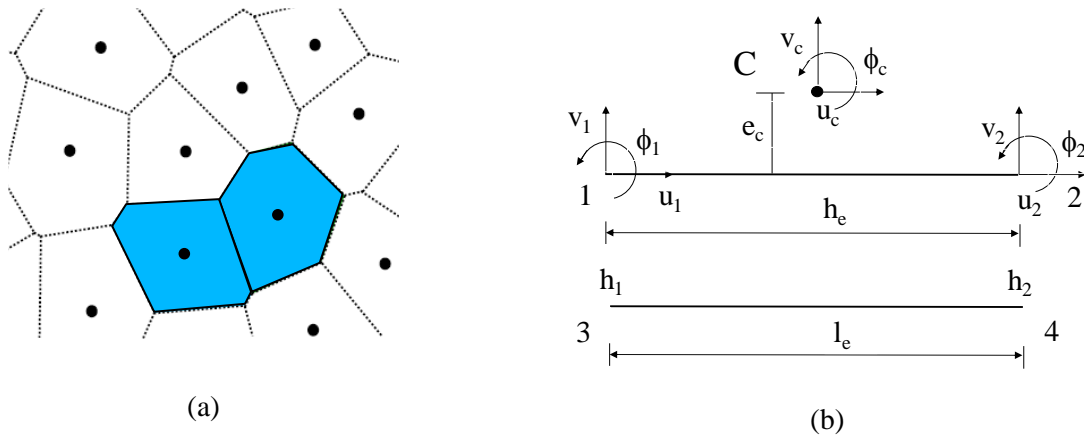
Figure 1. Example of (a) Voronoi tessellation and Delaunay triangulation; (b) Delaunay triangulation, degrees of freedom of the lattice elements for the mechanical and transport model in the local co-ordinate system.

The displacement of the mid-point C is defined in terms of the node DOF as follows:

$$u_c = B u_e \tag{1}$$

where:

$$u_e = \{u_1, v_1, \phi_1, u_2, v_2, \phi_2\}^T \; ; \; u_c = \{u_c, v_c, \phi_c\}^T \tag{2}$$

$$B = \begin{bmatrix} -1 & 0 & e_c & 1 & 0 & -e_c \\ 0 & -1 & -h_e/2 & 0 & 1 & -h_e/2 \end{bmatrix} \tag{3}$$

where h_e is the length of the element, e is eccentricity of the mid-point, l_e is the length of transport element. Then, the displacement u_c is replaced by deformation $\varepsilon = u_c / h_e = (\varepsilon_n, \varepsilon_s, \varepsilon_\varphi)$. The rigid matrix K of lattice element is determined by:

$$K = \frac{l_e \times t}{h_e} B^T D_e B \tag{4}$$

Where D_e is the elastic stiffness matrix and t is the out-plan thickness

The evolution of damage is controlled by stress-crack opening curve so that the mechanical response is independent of the length of lattice element used:

$$\sigma = (1-\kappa)D_e\varepsilon = (1-\kappa)\bar{\sigma} \tag{5}$$

Where elastic stress $\bar{\sigma} = D_e\varepsilon$ and κ is the damage variable, which can be determined by equation:

$$\left(1-\kappa\right)\varsigma = \frac{f_c}{f_t}\varepsilon_0 \exp\left(-\frac{h_e d\varsigma}{G_{fi}/f_i}\right) \quad (i=c,t) \tag{6}$$

Where $D_e = \begin{bmatrix} E & 0 & 0 \\ 0 & \gamma E & 0 \\ 0 & 0 & E \end{bmatrix}$, E is the Young's modulus, ς is history variable, $i=c$ (compression) or t (tension), G_{fc} and G_{ft} are fracture energies of pure compression and of pure tension, respectively.

2.2 Moisture transport lattice model

The moisture transport conduit elements are idealized as 1D conductive pipes (Figure 1) placed along the facets of the Voronoi polygons and their cross-sectional areas are calculated from the length of the corresponding edges of the dual Delaunay triangles. The moisture transport in concrete is simulated by the nonlinear equation derived based on Fick's law (Xi et al., 1994), which accounts for the transfer of both liquid and vapor phases, as follows:

$$\frac{dw}{dh}\frac{dh}{dt} - \nabla \cdot ((D_h)\nabla h) = 0 \tag{7}$$

Where w is the moisture content [kg/m³], D_h is moisture diffusivity of the undamaged material which is commonly defined in function of the relative humidity h as follows [25]:

$$D_h = D_1\left[\alpha_0 + (1-\alpha_0)/\left(1+\left(\frac{1-h}{1-h_c}\right)^n\right)\right] \tag{8}$$

where: D_1 is moisture diffusivity at full saturation [kg/m/s], α_0 is the ratio between the minimum and maximum moisture diffusivity, h_c is the relative humidity in middle of transition between

low and high diffusivity, n controls the slope of the moisture diffusivity transition. To consider the damage effect on the diffusivity, the latter is decomposed in 2 parts, one from material undamaged, and another one is taken in account the damaged material [26] as follows:

$$D_e(h, \tilde{\omega}_c) = D_h(h) + D_c(h_e, \tilde{\omega}_c)$$ (9)

Where $D_c(h_e, \tilde{\omega}_c)$ strongly depends on the modeled problem. In this present work, $D_c(h_e, \tilde{\omega}_c)$ is defined as linearly proportional to the crack opening, and determined by (Grassl, 2009) as:

$$D_c(h_e, \tilde{\omega}_c) = D_h(h) \frac{\tilde{\omega}_c}{\omega_{fk}}$$ (10)

where $\tilde{\omega}_c$ is an equivalent crack opening defined from the permanent and reversible deformation as explained in [26], and $\omega_{fk} = h_e \cdot \varepsilon_{fk}$ is a parameter which controls the slope of the change of the diffusivity, h_e is the mechanical element length which is here introduced to regularize the numerical results with respect the element size. For instance, in a previous work on normal concrete ε_{fk} was set to 0.25%. [26]. As proposed in the work of [25], $k = dw/dh$ is called the slope of the isotherm (or moisture) capacity, which can be simplified as a constant. In the present work, we assumed a simplified isotherm proposed by Kunzel which is a simplified adaptation of the BET model [28]–[30] as follows:

$$w = w_f \frac{(b-1)h}{b-h} \rightarrow \frac{dw}{dh} = \frac{w_f(b-1)b}{(b-h)^2}$$ (11)

where, w_f is a moisture content at the saturation (kg/m^3) and b is a dimensionless parameter greater than 1, typically b=1.3 [5]. This isotherm is a simplification of the moisture storage function which reproduces well more complex which are commonly employed in for cement based materials, such as law Van Genuchten model [31], in the capillary regime with relative humidity greater than 50%

2.3 Effect of damage on the adsorption isotherm

As a first simplified approach, the underlying idea of this work is to reproduce the reduction of the free water available in the capillary pores due to the formation of dry microcracks [7]. Thus, the water content decreases exponentially with the damage κ as follows:

$$w = w_f \frac{(b-1)h}{b-h} \exp(-c\kappa \frac{\varepsilon}{\varepsilon_{fk}})$$ (12)

where c and ε_{fk} are model parameter. Then, the moisture capacity reads:

$$\frac{dw}{dh} = w_f \frac{(b-1)b}{(b-h)^2} \exp\left(-c\kappa \frac{\varepsilon}{\varepsilon_{fk}}\right)$$ (13)

Figure 2a and Figure 2b show the moisture capacity and effect of damage parameter M, which is here defined as $M \equiv -c\kappa \dfrac{\varepsilon}{\varepsilon_{fk}}$, on the relative humidity h. The effect of damage is to reduce the water content in the adsorption isotherm. Note that M=0 represents the results of Kunzel (1995). Furthermore, Figure 2b shows the normalized moisture capacity $d(w/w_f)/dh$ versus the relative humidity h and the damage parameter M .

(a)	(b)
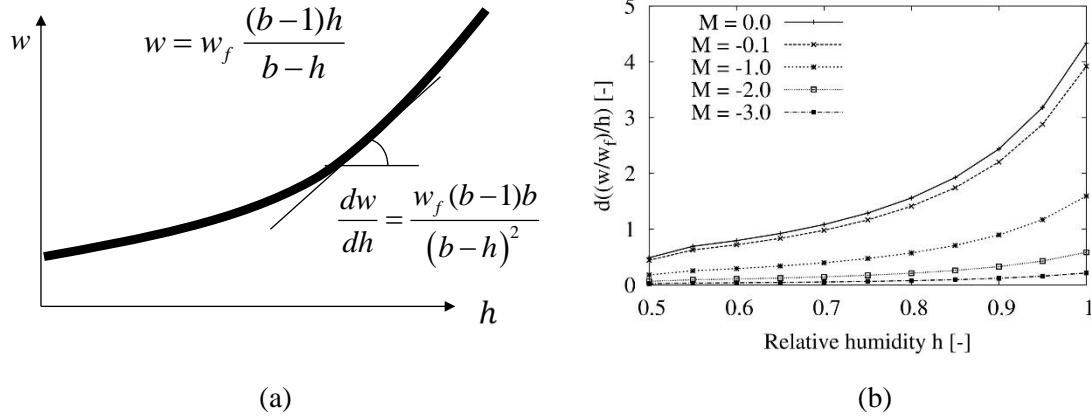
Figure 2. (a) Relation between water content and relative humidity, (b) Relation between the normalized moisture capacity vs. damage parameter M for different h values.

2.4. Hydro – mechanic - damage coupling model

Within a poromechanical framework [23], the overall stress is defined in function of the overall strain (ε) and the capillary pressure (P_c) as:

$$\sigma_c = (1-\kappa)D_e\varepsilon + b_l(1-\kappa)S_lP_c \tag{14}$$

Where κ is the damage parameter, b_l is the Biot coefficient, S_l is liquid saturation, and P_c is defined by Kelvin's law as:

$$P_c = -\frac{RT\rho_l}{W_m}\ln(h) \tag{15}$$

where:

R   : Perfect gas constant, R=8,314 J.K^{-1}.mol^{-1};

T   : Absolute temperature in Kelvin;

ρ_l : Density of the water, ρ_l =1000 kg.m^{-3};

W_m : Water molar mass, M=18.10^{-3} kg.mol^{-1};

3. RESULTS AND DISCUSSION

3.1. Static bending test

For validating the model, simulation results compared the flexural creep test for FRM-05 [12]. Moisture transfer model and mechanical parameters for material are presented in the Table 1.

Table 1: Moisture transfer model and mechanical parameters for material.

Material	Diffusivity parameters Eq.(8)				Isotherm parameters		Mechanical parameters				
	α_0 [-]	h_c [-]	n [-]	D_1 [kg/m/s]	w_f [kg/m^3]	b [-]	E [GPa]	f_c [GPa]	f_t [GPa]	G_{ft} [J/m^2]	G_{fc} [J/m^2]
FRM-05	0.05	0.74	16	8.5×10^{-8}	100	1.3	28	45	4	5×10^2	5×10^6
FRC-05	0.05	0.74	16	8.5×10^{-8}	100	1.3	31	52	5	5×10^2	6×10^6

The Figure 3a presents the mesh and boundary conditions for mechanical problem and the deformed mesh during the test, the boundary condition is identical to the experimentation but adding hygric condition, it means that specimen is submitted to both drying condition with relative humidity of 50%. The beam is initially loaded by displacement control until the crack opening reached the initial Crack Mouth Opening Displacement (CMOD), w0 (0.2 mm), then completely unloaded elastically, reloaded and subjected to sustained load conditions according to the test setup (80%) (Figure 3b). The crack opening and deflection will be measured in times.
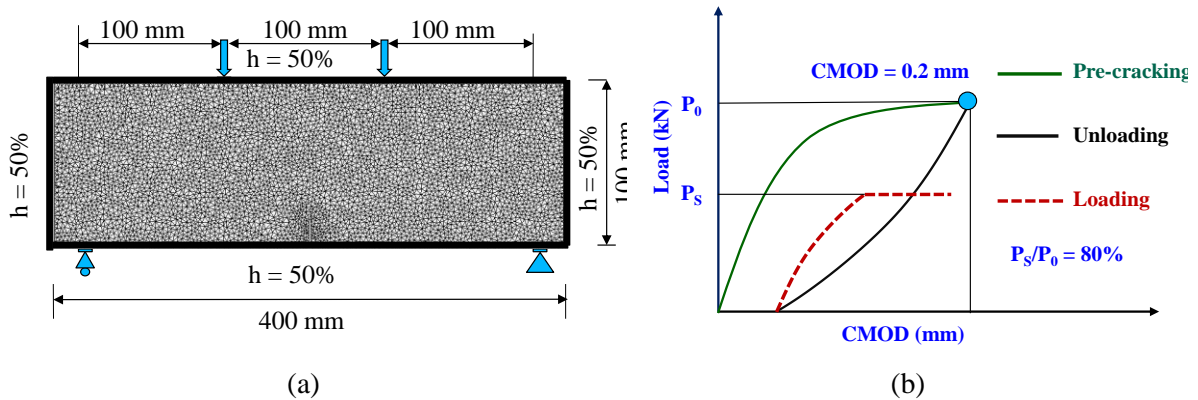
Figure 3. (a) Mesh, boundary and initial condition (b) Simulation procedure.

The crack opening-load curves are presented in Figure 4 for the numerical and experimental static responses. As a previously published model on the same experimental results [20]. It should be noted that the numerical model does not currently account for the unloading behavior as a purely damage model. However, the damage due to the loading is considered and the comparison between the numerical simulations and the experimental results will be made on the creep phase. All experimental flexural creep tests obtained by simulation show good agreement to the quasi-static experimental results [12]
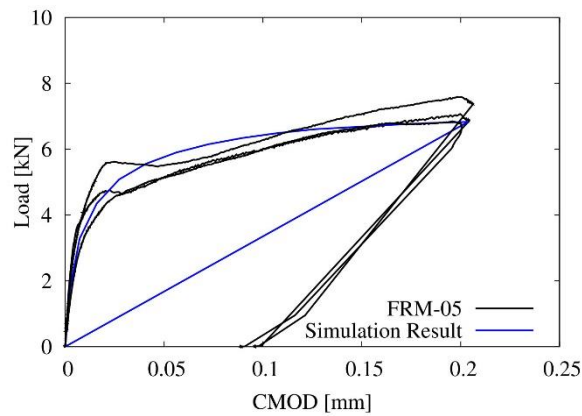
Figure 4. Crack opening-load responses of the experimental and numerical tests

3.2 Creep flexural behaviour

The experimental procedure for pre-cracking and applying the sustained load level of the flexural creep tests is presented in Figure 3b. The crack opening evolution in time at the high sustained load are presented in the Figure 5a, and Figure 7a. The simulated and experimental results show a good agreement in the crack propagation phase. One can note that, in the beginning of the bending test, due to the presence of a crack, creep increases significantly. This can be associated to macrocrack growth and a time-dependent propagation of the macrocrack. The pre-cracking caused the localisation of a macrocrack surrounded by microcracks, which is usually called fracture process zone. Once the sustained loading is applied, microcracks propagate over time around the crack tip zone. The discrete model proposed by [11] is always underestimated the amplitude of the crack opening while the lattice model seems to well capture.

(a)   (b)
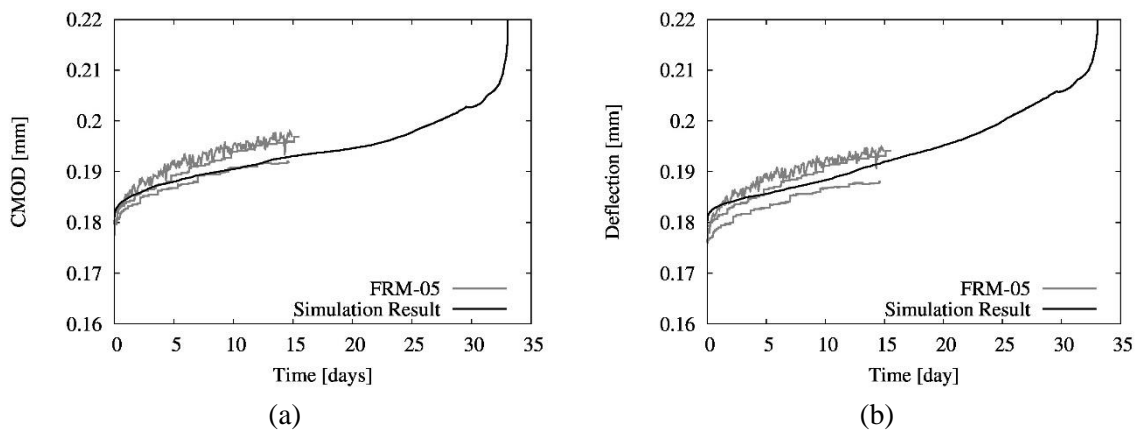
Figure 5. Comparison between simulated and experimental responses in terms of (a) crack opening vs time; (b) deflection vs. time.

The deflection-time responses of the flexural creep tests are presented in Figure 5b and Figure 7b. At high sustained loadings, the creep deflection evolution in time is the consequence of crack propagation. The formation of microcrack causes a redistribution of water in the capillary porosity. The consequent drying shrinkage strain occurs in the macrocrack tip, causing further microcrack growth. Furthermore, water can be transferred from the capillary pores to the macrocrack lips. Notably, the simple hypothesis of a damage effect on the adsorption isotherms of the proposed lattice model is able to simulate the first propagation initiation phase.

Effect of heterogeneity on the CMOD rate and deflection rate

The comparison of the CMOD rate and deflection rate for the experimental and simulation is presented in Figure 6 with a fairly acceptable with indication of the parity line (1:1). The simulation results for FRM-05 shows better agreement versus FRC-05. The model captures well the reduction of creep CMOD rate for the sample without large aggregate (FRM-05 vs. FRC-05).

(a)   (b)
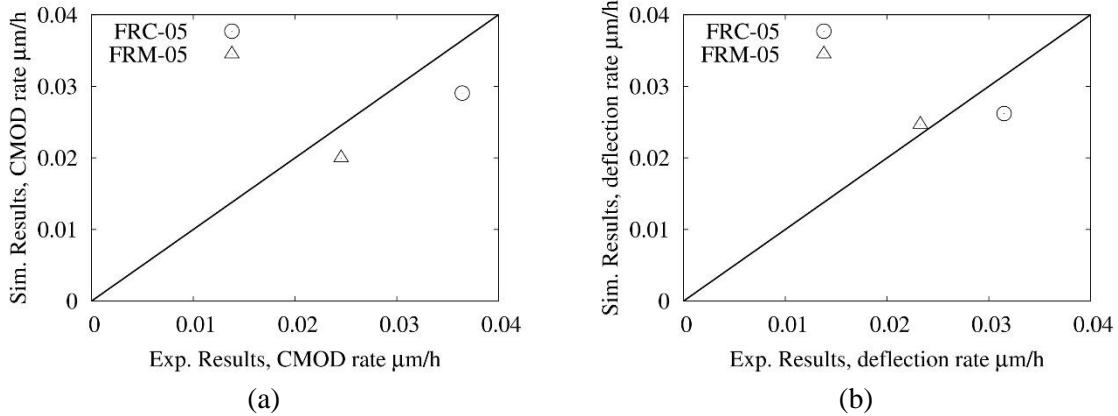
Figure 6. Comparison between simulated and experimental for the mix designs:
(a) CMOD rate; (b) Deflection rate.

Effect of parameters on the Creep flexural behavior

This section aims at studying the effect of the coefficient c in the Eq. (12) which affects the isotherm sorption. Figure 7a and Figure 7b show the effect of such coupling parameters on the time-evolution of the CMOD and deflection, respectively. The effect of c parameter is mostly on the creep rate is evident at the end of the secondary phase, before entering in the tertiary creep.

(a)   (b)
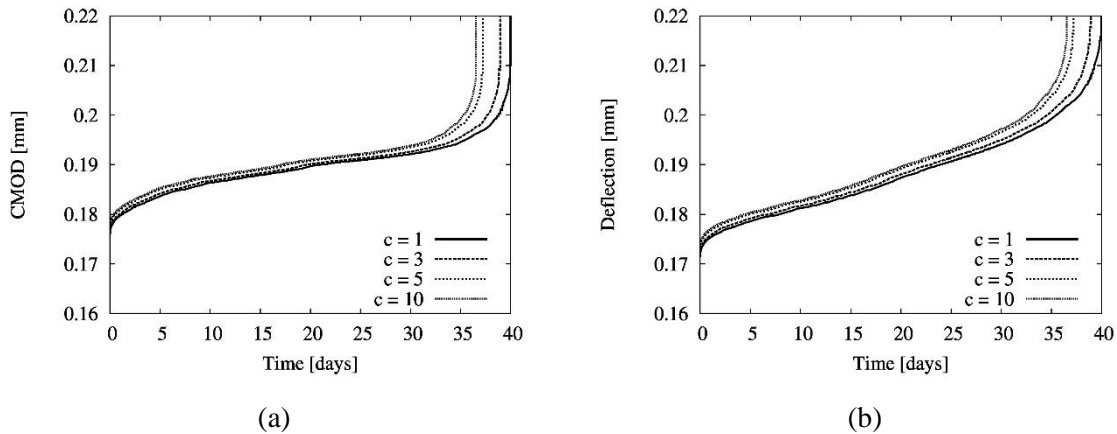
Figure 7. Effect of the coefficient c Eq. (12) on: (a) Crack opening ; (b) Deflection.

Finally, the effect of the coefficient ε_{fk} which govers the effect of damage on the water diffusion is also studied by a parametric analysis (Figure 8). Within the range of model parameters considered, the model indicated that the secondary creep rate seems governed by the diffusion rate, while the transition to tertiary creep is governed by the coupling term c.
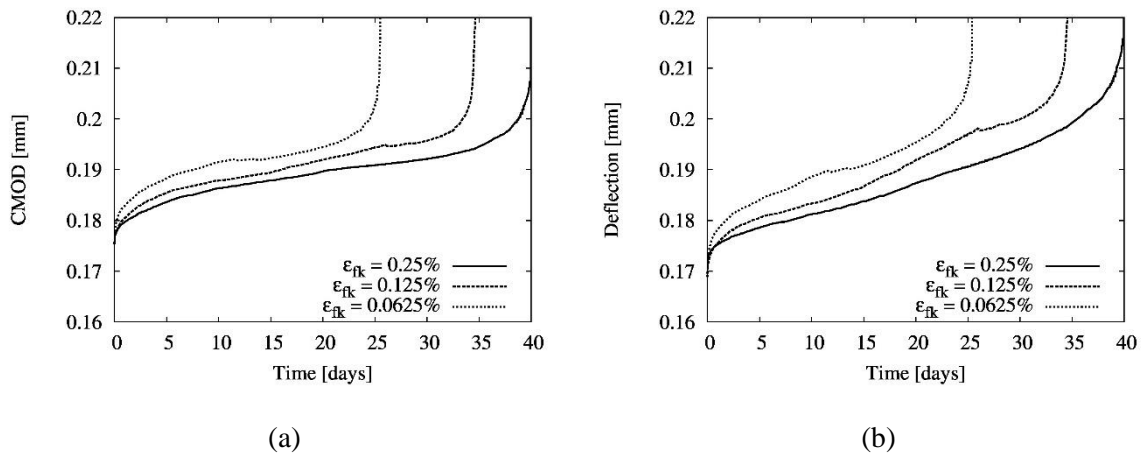
Figure 8. Effect of the coefficient ε_{fk} on: (a) Crack opening; (b) Deflection.

4. CONCLUSION

This work presented an original model to simply account for the effect of damage on the FRC secondary creep within a poromechanical framework. The hydro-damage couplings can engender microcrack process zone which govers the secondary creep of concrete at high stress. The model has been validated on 2D experiments of secondary creep on FRC which considers the effect of water-to-cement ratio and aggregate inclusion. Based on the present results, the following conclusions can be drawn:

1. With a reasonable and limited number of parameters, the proposed model assumed a simplified coupling between adsorption isotherm and damage, which allowed to fairly well predict the experimental secondary creep of FRM beams under sustained high loads. The model is based on a simplified assumption that cracking affect water moisture capacity, which can be related to water redistribution in the porosity systems due to microscopic cracks. The consequent hygral imbalance engenders the drying shrinkage, which, in zone under high stress, cause microcracking growth. This interactive process governs the crack growth rate associated to secondary creep of cement based composites.

2. The proposed model well predicted the effect of heterogeneity on the secondary creep rate, especially in terms of CMOD rate, which increased the microcracking growth due to the confining effect to the shrinkage strains.

3. The model validates the explanation of the secondary creep mechanisms proposed by Rossi et Acker, 1988 [9] for high sustained load which assumes a damage evolution driven by local drying shrinkage and water diffusion.

Future works are needed to enhance the poromechanical model towards more general applications. Eventually, the proposed model appears a powerful tool to assess the effect of microstructure heterogeneity on the secondary creep rate. Moreover, the model provides a first engineer tool for assessing the effect of secondary creep on the structural safety of aged and deteriorating concrete structures.

REFERENCES

[1]. A. M. Neville, W. H. Dilger, J. J. Brooks, Creep of plain and structural concrete. Construction press, 1983.

[2]. M.-Q. Thai, B. Bary, Q.-C. He, A homogenization-enriched viscodamage model for cement-based material creep, Eng. Fract. Mech., 126 (2014) 54–72. https://doi.org/ 10.1016/j.engfracmech.2014.04.021

[3]. A. M. Neville, Role of Cement in the Creep of Mortar, J. Proc., 55 (159) 963–984. https://doi.org/10.14359/11405.

[4]. F. Roll, Long-Time Creep-Recovery of Highly Stressed Concrete Cylinders, Spec. Publ., 9 (1964) 95–114. https://doi.org/10.14359/17221

[5]. Y. Xi, Z. P. Bažant, L. Molina, H. M. Jennings, Moisture diffusion in cementitious materials Moisture capacity and diffusivity, Adv. Cem. Based Mater., 1 (1994). https://doi.org/10.1016/1065-7355(94)90034-5

[6]. Claudio Mazzotti, Marco Savoia, Nonlinear creep, Poisson's ratio, and creep-damage interaction of concrete in compression, 99 (2002) 450-457. https://doi.org/10.14359/12323

[7]. P. Rossi, J.-L. Tailhan, F. Le Maou, L. Gaillet, E. Martin, Basic creep behavior of concretes investigation of the physical mechanisms by using acoustic emission, Cem. Concr. Res., 42 (2012) 61–73. https://doi.org/10.1016/j.cemconres.2011.07.011

[8]. Z. P. Bazant, G.-H. Li, Q. Yu, G. Klein, V. Kristek, Explanation of excessive long-time deflections of collapsed record-span box girder bridge in Palau, in Proc., 8th Int. Conf. on Creep, Shrinkage and Durability of Concrete and Concrete Structures, The Maeda Engineering Foundation, Ise-Shima, Japan, pp. 1–31, 2008.

[9]. P. Rossi, P. Acker, A new approach to the basic creep and relaxation of concrete, Cem. Concr. Res., 18 (1988) 799-803. https://doi.org/10.1016/0008-8846(88)90105-6

[10].P. Rossi, C. Boulay, J.-L. Tailhan, E. Martin, D. Desnoyers, Macrocrack propagation in concrete specimens under sustained loading: Study of the physical mechanisms, Cem. Concr. Res., 63 (2014) 98–104. https://doi.org/10.1016/j.cemconres.2014.05.006

[11].D. Daviau-Desnoyers, J.-P. Charron, B. Massicotte, P. Rossi, J.-L. Tailhan, Characterization of macrocrack propagation under sustained loading in steel fibre reinforced concrete, Mater. Struct., 49 (2015) 969–982. https://doi.org/10.1617/s11527-015-0552-3

[12]. T. Pham Duc, T. Tran Manh, T. Dang Trung, N. Vu Minh, N. Vu Minh, S. Luca, Experimental investigation of the secondary creep of fiber reinforced concrete at high stress: Macroscopic measurement and digital image correlation, Journal of Science and Technology in Civil Engineering, 16 (2022) 19–28.

[13]. Z. P. Bazant, S. Prasannan, Solidification Theory for Concrete Creep. I: Formulation, J. Eng. Mech., 115 (1989) 1691–1703. https://doi.org/10.1061/(ASCE)0733-9399(1989)115:8(1691)

[14]. M. Fernandez Ruiz, A. Muttoni, P. G. Gambarova, Relationship between nonlinear creep and cracking of concrete under uniaxial compression, J. Adv. Concr. Technol., 5 (2007) 383–393.

[15]. Z. P. Bazant, Y. Xiang, Crack growth and lifetime of concrete under long time loading, J. Eng. Mech., 123 (1997) 350–358.

[16]. C. Mazzotti, M. Savoia, Nonlinear creep damage model for concrete under uniaxial compression, J. Eng. Mech., 129 (2003) 1065–1075.

[17]. N. Reviron, F. Benboudjema, J. M. Torrenti, G. Nahas, A. Millard, Coupling between creep and cracking in tension, in 6th International Conference on Fracture Mechanics of Concrete and Concrete Structures, Italie, 2007.

[18]. D. Daviau-Desnoyers, Caractérisation et modélisation de l'évolution de la fissuration des bétons renforcés de fibres sous charge soutenue, Université Paris-Est, 2015.

[19]. J.-L. Tailhan, P. Rossi, D. Daviau-Desnoyers, Probabilistic numerical modelling of cracking in steel fibre reinforced concretes (SFRC) structures, Cem. Concr. Compos., 55 (2015) 315–321.

[20]. P. Rossi and S. Richer, Numerical modelling of concrete cracking based on a stochastic approach, Mater. Struct., 20 (1987) 334–337.

[21]. T. Pham Duc, T. Tran Manh, T. Dang Trung, N. Vu Minh, N. Vu Minh, S. Luca, Experimental investigation of the secondary creep of fiber reinforced concrete at high stress: Macroscopic measurement and digital image correlation, Journal of Science and Technology in Civil Engineering, 16 (2022) 19–28.

[22]. D. Daviau-Desnoyers, J.-P. Charron, B. Massicotte, P. Rossi, J.-L. Tailhan, Influence of Reinforcement Type on Macrocrack Propagation under Sustained Loading in Steel Fibre Reinforced Concrete, Struct. Concr., 17 (2016) 736-746, https://doi.org/10.1002/suco.201500069

[23]. D. T. Pham, L. Sorelli, M. Fafard, M.-N. Vu, Hydromechanical couplings of reinforced tensioned members of steel fiber reinforced concrete by dual lattice model, Int. J. Numer. Anal. Methods Geomech., 45 (2021). https://doi.org/10.1002/nag.3148

[24]. Y. Xi, Z. P. Bažant, L. Molina, H. M. Jennings, Moisture diffusion in cementitious materials Moisture capacity and diffusivity, Adv. Cem. Based Mater., 1 (1994) 258–266. https://doi.org/10.1016/1065-7355(94)90034-5

[25]. Z. P. Bažant, L. J. Najjar, Nonlinear water diffusion in nonsaturated concrete, Matér. Constr., 5 (1972) 3–20. https://doi.org/10.1007/BF02479073

[26]. P. Grassl, A lattice approach to model flow in cracked concrete, Cem. Concr. Compos., 31 (2009) 454–460. https://doi.org/10.1016/j.cemconcomp.2009.05.001

[27]. P. Grassl, A lattice approach to model flow in cracked concrete, Cem. Concr. Compos., 31 (2009) 454–460.

[28]. S. Brunauer, P. H. Emmett, E. Teller, Adsorption of gases in multimolecular layers, J. Am. Chem. Soc., 60 (1938) 309–319.

[29]. H. Klopfer, Water Transport in Solids by Diffusion, Bauverlag GmbH Wiesb. Berl., 1974.

[30]. Hartwig M.Kunzel, Similtaneous Heat and Moisture Transport in Building Component, Fraunhofer IRB Verl. Suttgart, 1995.

[31]. Van Genuchten, A Closed-form Equation for Predicting the Hydraulic Conductivity of Unsaturated Soils, Soil Science Society of America, 44 (1980) 892-898.

[32].Hartwig M.Kunzel, Similtaneous Heat Moisture Transport in Building Component, Fraunhofer IRB Verl. Suttgart, 1995.